ARTICLES

Journal of Semiconductors
(2020) 41, 032103
doi: 10.1088/1674-4926/41/3/032103

Influence of self-heating on the millimeter-wave and terahertz performance of MBE grown silicon IMPATT diodes

S. J. Mukhopadhyay[1], Prajukta Mukherjee[2], Aritra Acharyya[3, †], and Monojit Mitra[1]

[1]Department of Electronics and Telecommunication Engineering, Indian Institute of Engineering Science and Technology, West Bengal – 711103, India

[2]Department of Electrical Engineering, Cooch Behar Government Engineering College, West Bengal – 736170, India

[3]Department of Electronics and Communication Engineering, Cooch Behar Government Engineering College, West Bengal – 736170, India

Abstract: The influence of self-heating on the millimeter-wave (mm-wave) and terahertz (THz) performance of double-drift region (DDR) impact avalanche transit time (IMPATT) sources based on silicon (Si) has been investigated in this paper. The dependences of static and large-signal parameters on junction temperature are estimated using a non-sinusoidal voltage excited (NSVE) large-signal simulation technique developed by the authors, which is based on the quantum-corrected drift-diffusion (QCDD) model. Linear variations of static parameters and non-linear variations of large-signal parameters with temperature have been observed. Analytical expressions representing the temperature dependences of static and large-signal parameters of the diodes are developed using linear and 2nd degree polynomial curve fitting techniques, which will be highly useful for optimizing the thermal design of the oscillators. Finally, the simulated results are found to be in close agreement with the experimentally measured data.

Key words: IMPATT oscillators; linear temperature coefficient; self-heating; thermal runway; quadratic temperature coefficient

Citation: S J Mukhopadhyay, P Mukherjee, A Acharyya, and M Mitra, Influence of self-heating on the millimeter-wave and terahertz performance of MBE grown silicon IMPATT diodes[J]. *J. Semicond.*, 2020, 41(3), 032103. http://doi.org/10.1088/1674-4926/41/3/032103

1. Introduction

Impact avalanche transit time (IMPATT) oscillators are the most powerful solid state sources for generating microwave (3–30 GHz), mm-wave (30–300 GHz) and terahertz (0.3–10.0 THz) frequencies with sufficiently high power and high DC to RF conversion efficiency[1–7]. Si is the most convenient base material for IMPATT source, which is capable of delivering RF power up to 0.5 THz[8]. However some other semiconductors like GaAs, InP, 4H-SiC, wurtzite (Wz)-GaN, type-IIb diamond and also some heterostructures based on GaN–AlGaN, Si–SiC, GaAs–AlGaAs, etc. have shown immense potential as the base material of IMPATT sources operating in the mm-wave and THz (0.3–10.0 THz) frequency regime[9–17]. However, due to the availability of most advanced process technology, Si is still preferred over all other materials for the fabrication of IMPATT diodes. In 1987, Luy *et al.* fabricated double-drift region (DDR) Si IMPATT diodes via the molecular-beam epitaxy (MBE) technique for 94 GHz operation[18]. They obtained a maximum power of 600 mW with a 6.7% efficiency at 94 GHz; however, the device structures they used for fabrication and testing were un-optimized. Later, in 1990, Dalle *et al.* reported a 500 mW power output from flat-profile DDR Si IMPATT source at 94 GHz with optimized structural design[19]. Wollitzer *et al.* obtained around 225 mW RF power from flat profile DDR Si IMPATT source operating at 140 GHz[20]. Therefore, at the atmospheric window frequencies 94 and 140 GHz, DDR Si IMPATT sources have already shown extraordinary RF performance. However, at a higher atmospheric window, i.e. at 220 GHz, the experimentally obtained power output is only 50 mW[5]. This drastic decrease in power output from 140 to 220 GHz diminishes the potential of Si as a base material of IMPATT diodes designed to operate at higher mm-wave frequencies (> 220 GHz)[8]. The low power output from Si IMPATT source at 220 GHz obtained by Midford *et al.* in 1979 may have been caused by a lack of matured process technology of that time, a lower quality of Si substrate used, un-optimized structural design, defect in packaging, mismatch between the diode and passive circuitry, etc.[5].

One major problem with IMPATT oscillators is the self-heating of the diode under reverse bias during oscillating condition, as a result of the high current passing through it. Self-heating of the diode under oscillating condition raises the junction temperature well above room temperature (i.e. $T > 300$ K). This fact may cause thermal runaway followed by burnout of the device, if the temperature rises beyond the burnout temperature of the base material (which is around $T_B \approx 575$ K for Si). In order to avoid burnout as a result of self-heating of the diode, it must be mounted on an appropriately designed heat sink made of either metal (copper or silver) or type-IIa diamond[5]. In 2013, Acharyya *et al.* carried out a detailed thermal analysis of DDR Si IMPATT oscillators designed to operate at mm-wave atmospheric window frequencies such as 94, 140 and 220 GHz and at two different THz frequencies; 0.3 and 0.5 THz[21]. The heat sinks designed by Acharyya *et al.* are capable of keeping the junction temperature of the diodes fixed at around 500 K during the steady-

Correspondence to: A Acharyya, ari_besu@yahoo.co.in
Received 12 AUGUST 2019; Revised 24 AUGUST 2019.

Table 1. Optimized design parameters.

f_d (GHz)	W_n (μm)	W_p (μm)	N_D (10^{23} m^{-3})	N_A (10^{23} m^{-3})	N_{n+} (10^{25} m^{-3})	N_{p+} (10^{25} m^{-3})	J_0 (10^8 A/m^2)	D_j (μm)
94	0.400	0.380	1.200	1.250	5.000	2.700	3.40	35.0
140	0.280	0.245	1.800	2.100	5.000	2.700	5.80	25.0
220	0.180	0.160	3.950	4.590	5.000	2.700	14.5	20.0
300	0.132	0.112	6.000	7.300	5.000	2.700	24.5	15.0
500	0.072	0.072	15.00	16.20	5.000	2.700	55.0	10.0

state oscillating condition, which is well below the burn out temperature of Si (i.e. 575 K)[21]. A change of junction temperature causes a significant amount of variations in both static (DC) as well as large-signal characteristics of IMPATT sources. The said variations were demonstrated by Acharyya *et al.* in 2013, by investigating the temperature dependence of large-signal parameters of a DDR Si IMPATT diode designed to operate at 94 GHz[22].

In the present paper, the authors have studied the influence of junction temperature on both DC and large-signal characteristics of DDR Si IMPATT diodes designed to operate at different mm-wave and THz frequencies. The operating frequencies of DDR Si IMPATT sources chosen for the present study are 94, 140, 220, 300 and 500 GHz. It has already been concluded from the avalanche response time based analysis carried out earlier by the authors that the upper cut-off frequency of DDR Si IMPATT source is around 500 GHz[8]. That is why, in the present work, the simulation study on the DDR Si IMPATT has been carried out up to its highest operating frequency, i.e. up to 500 GHz or 0.50 THz. A non-sinusoidal voltage excited (NSVE) large signal tool developed by the authors, based on the quantum-corrected drift-diffusion (QCDD) model have been used for this purpose[23]. The variations of DC and large-signal parameters of the diodes under consideration with temperature ranging from 300 to 550 K have been obtained from the simulation. Appropriate curve-fitting techniques have been used to formulate the mathematical expressions presenting the DC and large-signal parameters as functions of temperature; temperature coefficients associated with each parameter of the device have also been obtained. This comprehensive study which provides analytical expressions for each DC and large signal parameters of the device as functions of temperature will be highly useful for researchers to carry out thermal design of Si IMPATT oscillators operating at different mm-wave and THz frequencies.

2. Structure, material, fabrication and simulation

The descriptions of device structure and corresponding design parameters, material parameters associated with the base semiconductor (i.e. Si), fabrication process and simulation methodology have been presented in this section.

2.1. Structure

The DDR IMPATT diodes possess p^+–p–n–n^+ structure. The DDR diodes are more powerful and efficient than the single-drift region (SDR) diodes having either n^+–n–p^+ or p^+–p–n^+ structure due to the presence of two drift regions in DDR diodes (n- and p-drift regions for the drifting of electrons and holes, respectively) in comparison to the existence of only one drift region in SDR diodes (either n-drift region in n^+–n–p^+ structure for the drifting of electrons or p-drift region in p^+–p–n^+ structure for the drifting of holes). As a result of that, DDR diodes are always preferred over SDR diodes, though the fabrication of DDR IMPATT diodes is much more complex. The thickness of p^+, p, n, n^+ layers (W_{p+}, W_p, W_n, W_{n+}) and corresponding doping concentrations (N_{p+}, N_A, N_D, N_{n+}) of a diode operating at a particular frequency (f_d) are initially chosen using the transit time formula of Sze *et al.*[24]. In the next step, the initially chosen structural and doping design parameters as well as the bias current density (J_0) are optimized using the DC followed by large-signal simulation subject to obtain the maximum DC to RF conversion efficiency; the details of this optimization technique have already been discussed elsewhere[22]. The diameter of the mesa diodes at the junction region (D_j) have been chosen from the thermal analysis subject to obtain maximum RF power output by avoiding the burnout of the device[21]. The optimized design parameters of DDR Si IMPATT diodes designed to operate at different mm-wave and THz frequencies are given in Table 1.

2.2. Material

The electric field and temperature dependences of ionization rate of electrons and holes in Si have been incorporated in the NSVE large-signal simulation program via empirical relations fitted from the experimental data of Grant[25]. The same dependences of drift velocity of charge carriers in Si are included in the simulation tool using the empirical relations obtained via a curve fitting technique from experimentally measured data reported by Canali *et al.*[26]. Other important material parameters such as mobility, diffusion length, effective mass, diffusivity of charge carriers in Si are taken from recently published reports[27, 28]. Temperature dependence of bandgap in Si has been introduced by using the relation formulated from the experimental data of Varshni[29]. Other parameters like permittivity, density of states, effective mass of Si, effective density of states for electrons in conduction band and for holes in valence band, temperature dependent intrinsic carrier concentration in Si are taken from the published literature[27].

2.3. Fabrication

The (100) oriented n^+-type wafers having donor concentration of around ~10^{25} m^{-3} can be used as the substrate of mm-wave and THz diodes. Initially the wafer has to be cleaned using RCA etch, followed by Si-beam cleaning at around 850 °C[30, 31]. The n^+-substrate has to be thinned below the thickness of 10 μm using backside mechanical polishing followed by chemical etching using a diluted solution of KOH. Next the n-layer can be MBE grown on the substrate at a temperature of 750 °C; simultaneously during the growth, n-type doping can be achieved via doping by secondary implantation (DSI) technique using Sb as n-type impurities[32]. After the desired growth of n-epitaxial layer a flash-off step has to be performed for desorbing the Sb adlayer from the upper surface of the grown n-layer[33]. Over the n-layer, the p-lay-

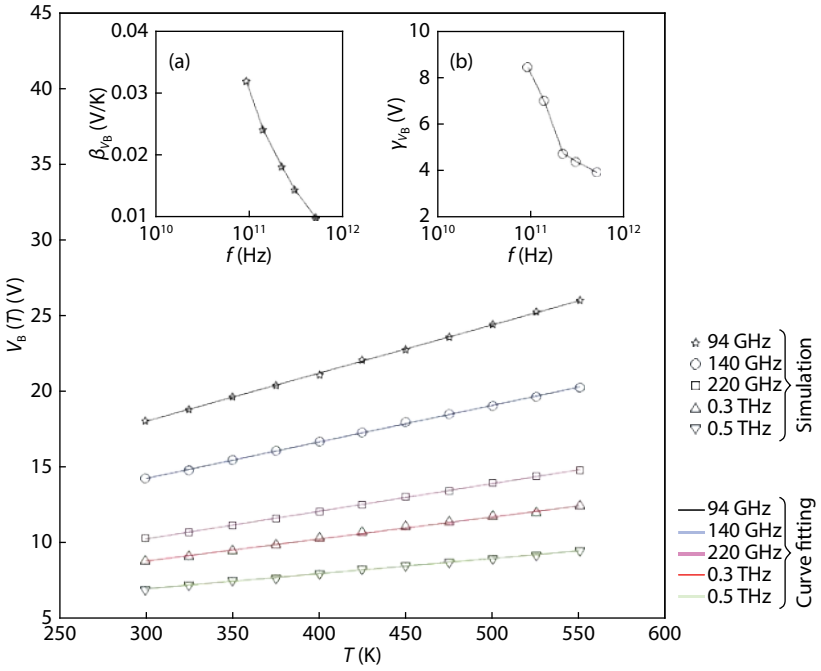

Fig. 1. (Color online) Variations of breakdown voltage of Si IMPATT sources operating at different mm-wave and THz frequencies with temperature; insets of the figure show (a) linear temperature coefficient of breakdown voltage, and (b) corresponding constant linear fitting parameter with operating frequency.

er can be MBE grown at 650 °C in which p-type doping of desired dosage can be achieved by Ga co-evaporation[34]. After the completion of the growth of p-epitaxial layer, again a flash-off process has to be performed in order to remove the Ga adlayer from the upper surface of the grown p-layer. The p^+-contact layer having doping concentration ~10^{25} m^{-3} can be grown on the p-epitaxial layer using the solid-phase-MBE (SP-MBE) technique followed by thermal annealing process of maximum 600 °C temperature[35]. The metallization on both p^+ and n^+-sides can be done via thermal evaporation of Ti followed by Au. The primary metal for forming the metal contacts is Au; the purpose of Ti is to resist Au atoms to migrate into p^+ and n^+-layers. Finally, the mesa diodes having desired junction diameters (Table 1) can be defined by standard photo-lithography technique and formed using chemical etching in a solution of HF and HNO_3.

2.4. Simulation

The NSVE large-signal simulation technique based on QCDD model has been used to study the effect of junction temperature on both DC and large signal characteristics of DDR Si IMPATT diodes designed to operate at different mm-wave and THz frequencies[23]. The design parameters and material parameters of Si as mentioned earlier are given as the inputs of the simulation tool prepared in in-house codes in MATLAB environment. The simulation tool provides important DC parameters like breakdown voltage ($V_B(T)$), avalanche zone voltage drop ($V_A(T)$), avalanche zone width ($x_A(T)$), etc. and significant large-signal parameters such as avalanche resonance frequency ($f_a(T)$), optimum frequency ($f_p(T)$), admittance characteristics $G(f,T)$ versus $B(f,T)$ plots, where G and B are conductance and susceptance of the device respectively, f is the frequency), RF power output ($P_{RF}(T)$) and DC to RF conversion efficiency ($\eta_L(T)$), as outputs as functions of temperature. The effects of quantum tunneling, quantum confinement (quantum mechanical phenomena are important for the diodes especially when the depletion layer thickness shrinks below the classical limiting length), band-to-band tunneling, trap-assisted tunneling, carrier diffusion, skin effect and parasitic series resistance have been incorporated in the simulation program[36–41].

3. Characteristics

It is already reported that DC to RF conversion efficiency of mm-wave and THz DDR Si IMPATT sources are considerably small (< 10%)[21]. Therefore a very small portion of input DC power (P_{DC}) is converted to RF power and a very large portion of that is dissipated as heat (> 90% of P_{DC}) within the diode. This dissipation of DC power within the device is the origin of the self-heating problem associated with IMPATT oscillators, which leads to a rise of the temperature[21]. On the other hand, it is already observed that the RF power output and conversion efficiency of the IMPATT sources are significantly improved if the diode temperature increases well above the room temperature[22]. This fact encourages the designers as well as researchers to keep the diode temperature (T) of the source fixed around 500 K via an appropriate heat sinking arrangement, which is well above room temperature as well as sufficiently smaller than the burnout temperature of Si (300 K < T < T_B = 575 K); therefore, it simultaneously ensures high RF power output from the source as well as safe and sustained continuous-wave (CW) operation of it[21]. Thus, the knowledge of the dependences of DC and large-signal parameters of DDR Si IMPATT diodes on temperature is essential for the thermal designing of the oscillators. In this section, the above mentioned dependences obtained from the NSVE large-signal simulation of mm-wave and THz DDR Si IMPATT diodes are presented and analyzed.

3.1. Static characteristics

The variations of DC breakdown voltage ($V_B(T)$) of the diodes with temperature have been shown in Fig. 1. The same

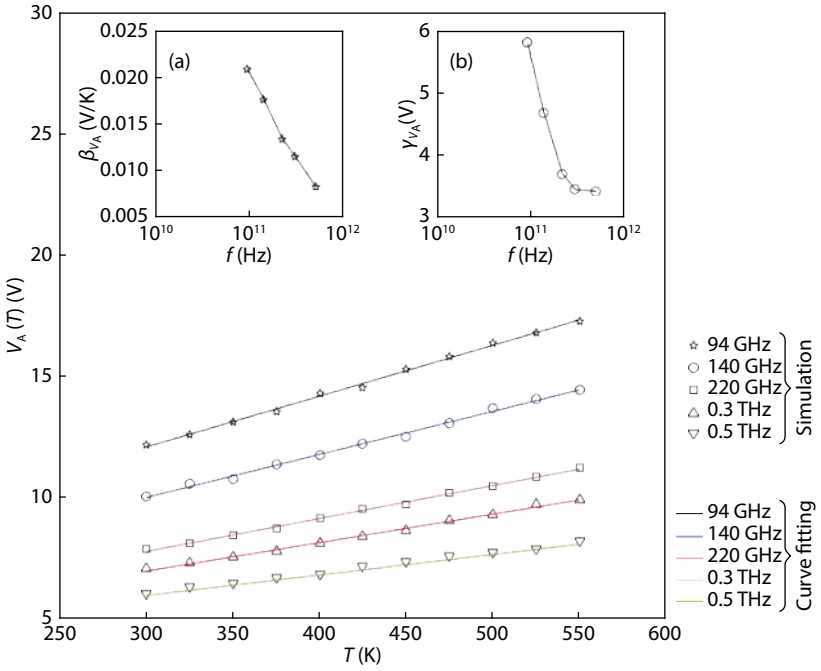

Fig. 2. (Color online) Variations of avalanche zone voltage drop of Si IMPATT sources operating at different mm-wave and THz frequencies with temperature; insets of the figure show (a) linear temperature coefficient of avalanche zone voltage drop and (b) corresponding constant linear fitting parameter with operating frequency.

variations of avalanche zone voltage drop ($V_A(T)$) and avalanche region width ($x_A(T)$) of the diodes are shown in Figs. 2 and 3 respectively. It is interesting to observe from Figs. 1–3 that the said variations of DC parameters with temperature are absolutely linear in nature and all have a positive slope. It is already reported by Grant that the ionization rate of charge carriers in Si decreases significantly with the increase of temperature[25]. Therefore, if one considers two temperatures T_1 and T_2, where $T_2 > T_1$, then the ionization rate of electrons and holes at T_2 will be smaller compared to those at T_1 for a given electric field. Therefore, at the temperature T_2 more electric field is required to generate the number of electron–hole pairs (EHPs) required to cause avalanche breakdown as compared to the required breakdown field at the temperature T_1. Consequently, breakdown voltage at T_2 will be greater than that at T_1. Moreover, at T_2 a broader mean free path is required by the charge carriers in order to generate the EHPs required for breakdown for a given electric field as compared to the mean free path required by the electrons and holes for generating the EHPs required for breakdown at T_1 at the same electric field. Therefore, at T_2, avalanche zone width will be broader and avalanche zone voltage drop will be higher compared to those at T_1. This discussion explains the causes of the increase of the DC parameters of the diodes under consideration with the increase of temperature.

Now, the relations expressing the dependences $V_B(T)$, $V_A(T)$ and $x_A(T)$ with temperature (T) will be formed. It is already observed from Figs. 1–3 that these dependences are linear in nature for all the diodes under consideration. The temperature dependences of a DC parameter can be expressed via the equation of a straight line given by

$$D(T) = \beta_D T + \gamma_D, \tag{1}$$

where $\beta_D = dD(T)/dT$ is the linear temperature coefficient associated with the DC parameter $D(T) \in \{V_B(T), V_A(T), x_A(T)\}$, $\gamma_D = D(T = 0)$ is the constant parameter associated with the linear fitting. Now, the linear temperature coefficients (β_{V_B}, β_{V_A}, β_{x_A}) and the constant fitting parameters (γ_{V_B}, γ_{V_A}, γ_{x_A}) of V_B, V_A and x_A are obtained using a linear curve fitting technique for all the diodes, and the variations of those with operating frequency have been illustrated in the corresponding insets of the Figs. 1–3. The value of β_D which is just the slope of $D(T)$ versus T curves are found to decrease drastically with the increase of frequency of operation. The β_{V_B} is found to be reduced from 3.175×10^{-2} to 1.001×10^{-2} V/K for the increment of operating frequency from 94 GHz to 0.5 THz; the same variations in β_{V_A} and β_{x_A} are found to be 2.094×10^{-2}–0.844×10^{-2} V/K and 0.288×10^{-2} – 0.066×10^{-2} μm/K, respectively. It can be concluded from the above observation that the temperature sensitivity of the DC parameters of DDR Si IMPATT diodes decreases with the increase of operating frequency; i.e. higher frequency diodes are less sensitive to temperature. On the other hand, the value of γ_D which indicates the hypothetical initial value of $D(T)$ at $T = 0$, are also observed to decrease with increase of the frequency of operation; it is obvious due to the smaller active layer thickness ($W_d = W_n + W_p$) of higher frequency diodes. The values of β_{V_B}, β_{V_A}, β_{x_A} and γ_{V_B}, γ_{V_A}, γ_{x_A} obtained from this analysis are listed in Table 2, which will be very useful for the thermal designers.

3.2. Large-signal characteristics

The variations of important large-signal parameters such as the avalanche resonance frequency ($f_a(T)$), optimum frequency ($f_p(T)$), peak negative conductance ($G_p(T)$), corresponding susceptance ($B_p(T)$), RF power output ($P_{RF}(T)$) and conversion efficiency ($\eta_L(T)$) of the diodes under consideration with temperature are shown in Figs. 4–9, respectively. All the above variations are observed to be non-linear in nature and

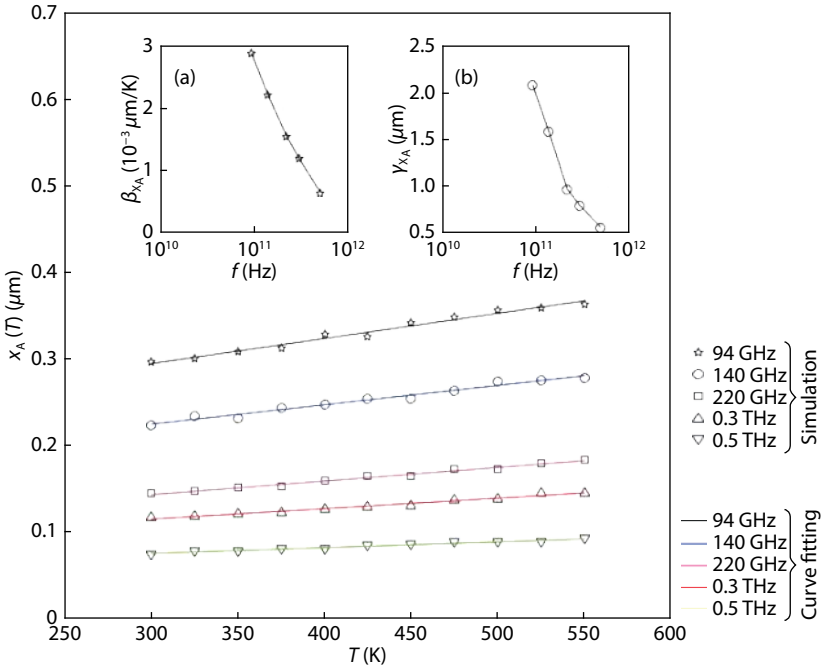

Fig. 3. (Color online) Variations of avalanche zone width of Si IMPATT sources operating at different mm-wave and THz frequencies with temperature; insets of the figure show (a) linear temperature coefficient of avalanche zone width and (b) corresponding constant linear fitting parameter with operating frequency.

Table 2. Linear temperature coefficient and constant fitting parameter associated with DC parameters for the temperature range 300–550 K.

f_d (GHz)	V_B (V)		V_A (V)		x_A (μm)	
	β_{V_B} (10^{-2} V/K)	γ_{V_B}(V)	β_{V_A} (10^{-2} V/K)	γ_{V_A}(V)	β_{x_A} (10^{-2} μm/K)	γ_{x_A} (μm)
94	3.175	8.481	2.094	5.821	0.288	2.082
140	2.482	7.007	1.772	4.711	0.222	1.586
220	1.824	4.788	1.356	3.734	0.156	0.975
300	1.452	4.453	1.171	3.482	0.120	0.803
500	1.001	3.978	0.844	3.555	0.066	0.571

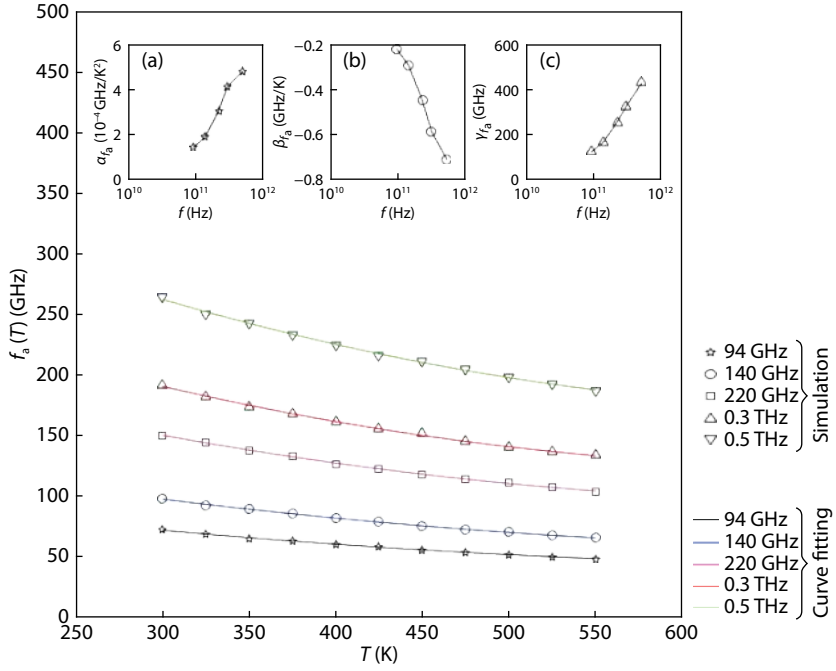

Fig. 4. (Color online) Variations of avalanche resonance frequency of Si IMPATT sources operating at different mm-wave and THz frequencies with temperature; insets of the figure show (a) quadratic temperature coefficient, (b) linear temperature coefficient of avalanche resonance frequency and (c) corresponding constant fitting parameter with operating frequency.

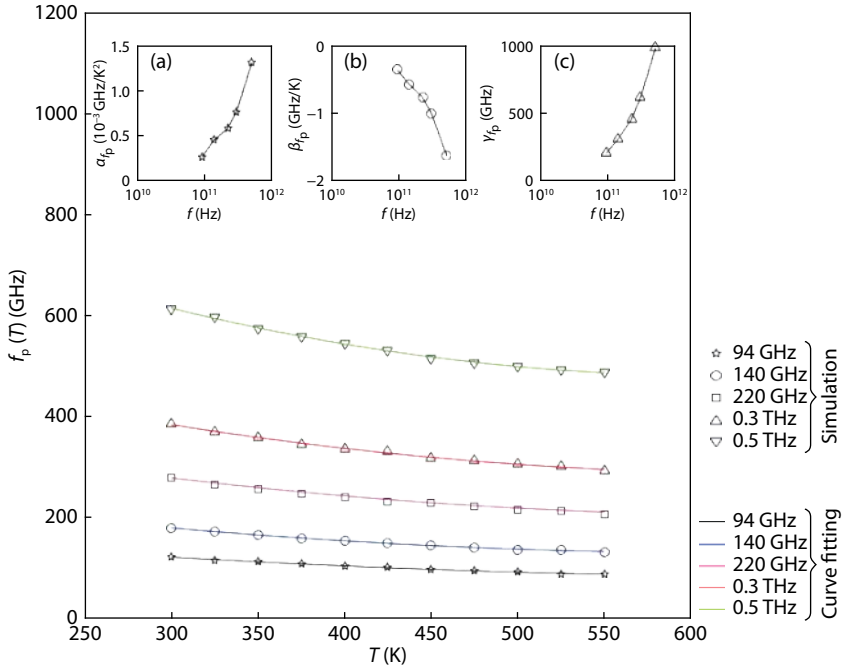

Fig. 5. (Color online) Variations of optimum frequency of Si IMPATT sources operating at different mm-wave and THz frequencies with temperature; the insets show (a) quadratic temperature coefficient, (b) linear temperature coefficient of optimum frequency and (c) corresponding constant fitting parameter with operating frequency.

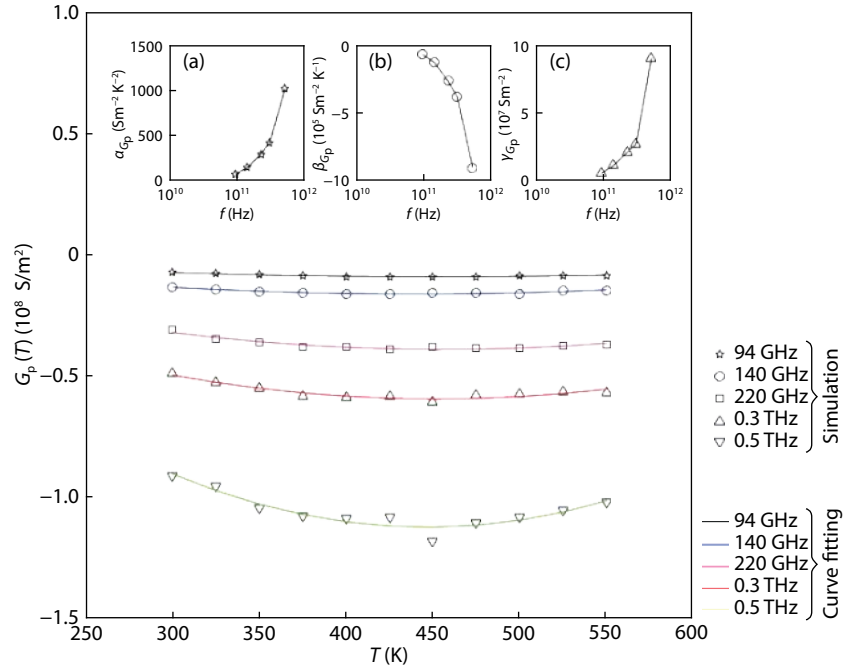

Fig. 6. (Color online) Variations of peak negative conductance of Si IMPATT sources operating at different mm-wave and THz frequencies with temperature; insets of the figure show (a) quadratic temperature coefficient, (b) linear temperature coefficient of peak negative conductance and (c) corresponding constant fitting parameter with operating frequency.

can be fitted using a quadratic polynomial equation given by

$$L(T) = \alpha_L T^2 + \beta_L T + \gamma_L, \quad (2)$$

where $\alpha_L = (1/2)(d^2L(T)/d^2T)$ is the quadratic temperature coefficient, $\beta_L = dL(T)/dT$ is the linear temperature coefficient of the large-signal $L(T) \in \{f_a(T), f_p(T), G_p(T), B_p(T), P_{RF}(T), \eta_L(T)\}$ parameter, $\gamma_L = L\ (T = 0)$ is the constant fitting parameter of the large-signal parameter $L(T)$. Now, the values of α_L, β_L and γ_L for all the diodes are calculated via the 2nd degree polynomial or quadratic polynomial fitting technique.

The variations of α_L, β_L and γ_L associated with all large-signal parameters with the frequency of oscillation have been shown in the insets of the corresponding figures. It is interesting to note that the quadratic temperature coefficients of f_a, f_p, G_p, P_{RF} and η_L are found to be positive and monotonically increasing with frequency of operation; whereas it is observed to be negative and monotonically decreasing with the frequency of operation for the parameter B_p. However, the lin-

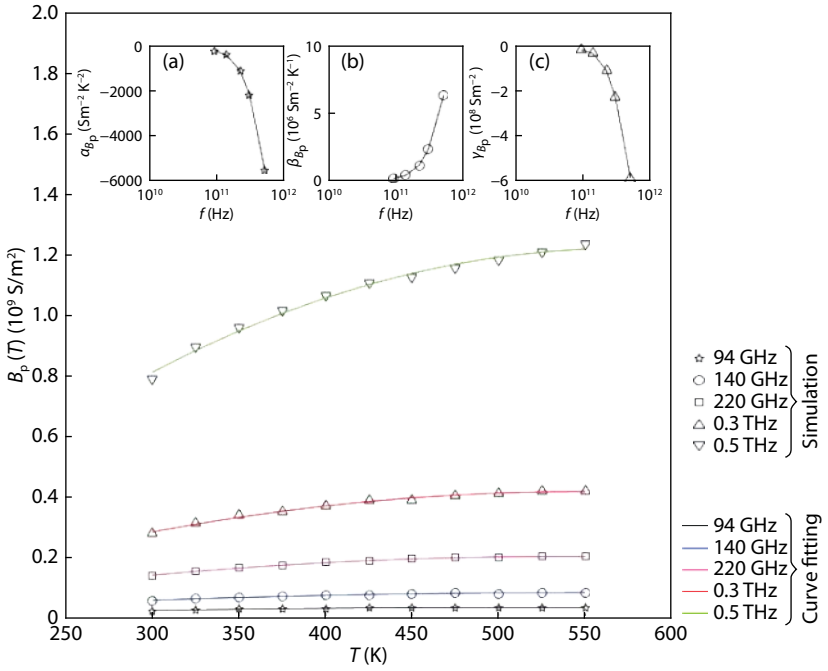

Fig. 7. (Color online) Variations of susceptance corresponding to the peak negative conductance of Si IMPATT sources operating at different mm-wave and THz frequencies with temperature; insets of the figure show (a) quadratic temperature coefficient, (b) linear temperature coefficient of susceptance corresponding to the peak negative conductance and (c) corresponding constant fitting parameter with operating frequency.

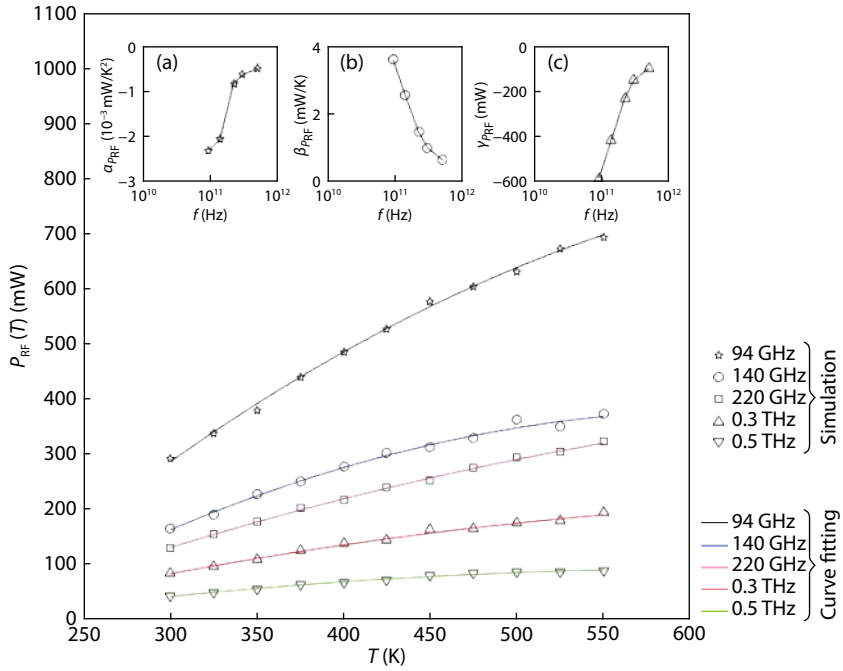

Fig. 8. (Color online) Variations of RF power output of Si IMPATT sources operating at different mm-wave and THz frequencies with temperature; insets of the figure show (a) quadratic temperature coefficient, (b) linear temperature coefficient of RF power output and (c) corresponding constant fitting parameter with operating frequency.

ear temperature coefficients of f_a, f_p and G_p are found to be negative and monotonically decreasing with frequency, while it is found to be positive and monotonically increasing with frequency for B_p and positive but monotonically decreasing for P_{RF} and η_L. It is also noteworthy that the constant fitting parameters of different large-signal parameters have a different sign (either positive or negative) and possess a different nature of variation with frequency (either monotonically increasing or decreasing with frequency). The values of α_L, β_L and γ_L associated with all the large-signal parameters of the diodes under consideration are listed in Tables 3 and 4. Again, the datasets presented in Tables 3 and 4 will be very useful for carrying out the optimum thermal design of mm-wave and THz DDR Si IMPATT oscillators.

3.3. Validation of simulation results

The variations of experimentally measured power output of DDR Si IMPATT sources reported by Luy *et al.* at 94 GHz, Wollitzer *et al.* at 140 GHz and Midford *et al.* at

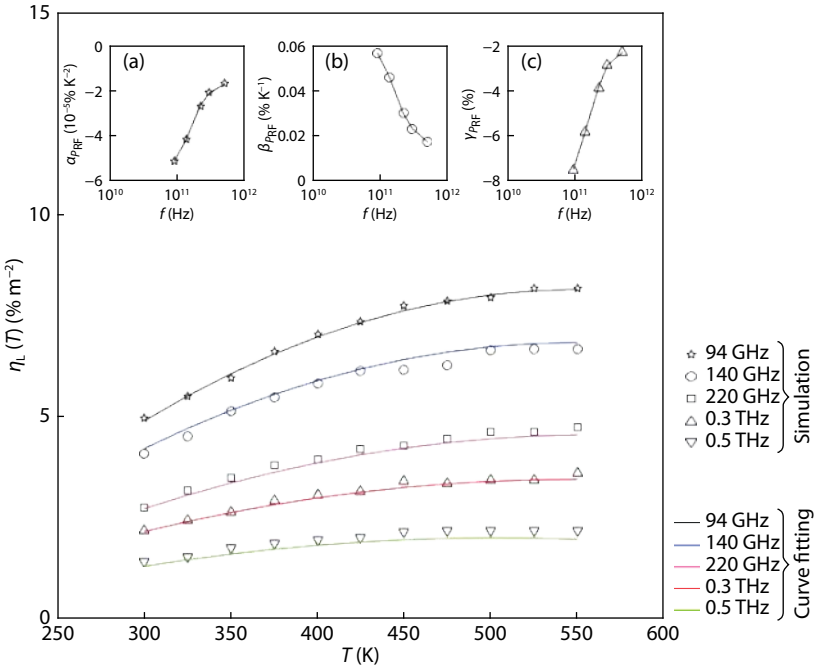

Fig. 9. (Color online) Variations of DC to RF conversion efficiency of Si IMPATT sources operating at different mm-wave and THz frequencies with temperature; insets of the figure show (a) quadratic temperature coefficient, (b) linear temperature coefficient of DC to RF conversion efficiency and (c) corresponding constant fitting parameter with operating frequency.

Table 3. Quadratic temperature coefficient, linear temperature coefficient and constant fitting parameter associated with large-signal parameters such as f_a, f_p and G_p for the temperature range of 300–550 K.

	f_a (GHz)			f_p (GHz)			G_p (S/m^2)		
f_d (GHz)	α_{f_a} (10^{-4} GHz/K^2)	β_{f_a} (GHz/K)	γ_{f_a} (GHz)	α_{f_p} (10^{-4} GHz/K^2)	β_{f_p} (GHz/K)	γ_{f_p} (GHz)	α_{G_p} (S/(m^2·K^2))	β_{G_p} (10^4 S/(m^2·K))	γ_{G_p} (10^6 S/m^2)
94	1.445	–0.216	124.33	2.595	–0.357	206.61	71.72	–6.500	5.550
140	1.900	–0.289	167.75	4.499	–0.569	310.50	141.24	–12.442	11.128
220	3.041	–0.442	256.00	5.772	–0.766	455.20	287.81	–26.236	20.759
300	4.151	–0.581	327.98	7.670	–1.005	616.69	422.28	–38.183	26.985
500	4.798	–0.706	431.23	13.093	–1.623	983.08	1014.40	–90.641	90.544

Table 4. Quadratic temperature coefficient, linear temperature coefficient and constant fitting parameter associated with large-signal parameters such as B_p, P_{RF} and η_L for the temperature range of 300–550 K.

	B_p (S/m^2)			P_{RF} (mW)			η_L (%)		
f_d (GHz)	α_{B_p} (S/(m^2·K^2))	β_{B_p} (10^5 S/(m^2·K))	γ_{B_p} (10^7 S/m^2)	$\alpha_{P_{RF}}$ (10^{-3} mW/K^2)	$\beta_{P_{RF}}$ (mW/K)	$\gamma_{P_{RF}}$ (mW)	α_{G_p} (10^{-5} %K^{-2})	β_{η_L} (%K^{-1})	γ_{η_L} (%)
94	–206.19	2.151	–1.910	–2.290	3.590	–584.66	–5.158	0.0568	–7.500
140	–399.27	4.397	–3.531	–2.040	2.555	–420.05	–4.185	0.0460	–5.817
220	–1090.30	1.173	–11.023	–0.830	1.461	–232.86	–2.674	0.0300	–3.858
300	–2156.80	2.367	–22.985	–0.640	0.970	–150.32	–2.101	0.0230	–2.839
500	–5516.30	6.314	–58.475	–0.500	0.616	–97.89	–1.687	0.0170	–2.269

220 GHz, along with the power output of all mm-wave and THz sources under consideration obtained from simulation with frequency are shown in Fig. 10; all of these experimental measurements and simulations have been carried out near 500 K[5, 18, 20]. It is observed from Fig. 10 that the large-signal simulation results presented in this paper as regards RF power output are in very close agreement with the experimentally measured data except at 220 GHz; the probable causes of the discrepancy found at 220 GHz have already been mentioned in the introduction section. Moreover, the variation of DC to RF conversion efficiency of the sources obtained from simulation with frequency has been shown in the inset of Fig. 10; experimentally measured DC to RF conversion efficiency of the source reported by Luy *et al.* at 94 GHz is also shown in the said inset[18]. It is observed that in this case also the agreement between the simulated and measured data at 94 GHz is quite reasonable.

There are similar studies based on the temperature analysis of DDR IMPATT oscillators based on other semiconductors like some conventional narrow bandgap (NBG) semiconduct-

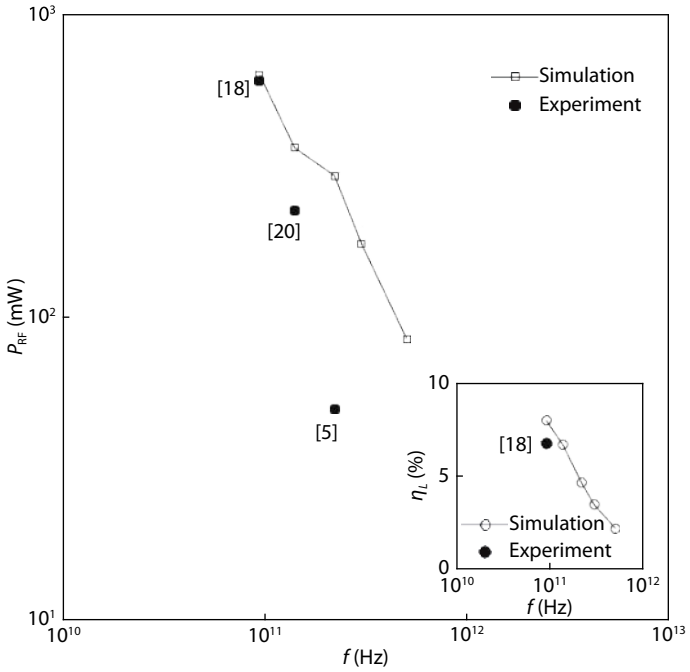

Fig. 10. Variations of RF power output of Si IMPATT sources obtained from the large-signal simulation and experimental measurements[5, 18, 20] at 500 K with operating frequency; inset shows the variations of DC to RF conversion efficiency of the sources obtained from the large-signal simulation and experimental measurement[18] at 500 K with operating frequency.

ors such as GaAs, InP, etc. and some wide bandgap (WBG) semiconductors such as 3C-SiC, 4H-SiC, 6H-SiC, Wz-GaN, type-IIb diamond, etc. using similar methodology adopted by the authors to carry out the present work; however, most the important criteria behind this will be the availability of experimentally measured temperature dependent material parameters of the above-mentioned semiconductors. Otherwise, the procedure described in this paper is generic for all base materials mentioned above. Moreover, similar studies can also be carried out for some other IMPATT diode structures like single-drift region (SDR), double-avalanche region (DAR) diodes. Especially, the temperature analysis of low noise DAR Si IMPATT will be very useful for future researchers due to the capability of a single DAR source to operate at multiple bands[42]; this study will be carried out in due course by the authors. Last but not the least, the description of the IMPATT sources cannot be completed without studying the avalanche noise performance of the source. Since, the IMPATT sources are inherently noisy, the effect of temperature variation on the noise performance of DDR Si IMPATT sources are very important to understand before finalizing the thermal design of the oscillator. That is why the authors plan to carry out a temperature dependent noise simulation of DDR Si IMPATT sources in due course.

4. Conclusion

The influence of self-heating on the mm-wave and THz performance of DDR Si IMPATT sources has been investigated in this paper. The dependences of static and large-signal parameters on junction temperature are estimated by using a NSVE large-signal simulation technique developed by the authors, which is based on the QCDD model reported earlier. Linear variations of static parameters and non-linear variations of large-signal parameters with temperature have been observed. Analytical expressions representing the temperature dependences of static and large-signal parameters of the diodes are developed using linear and quadratic polynomial curve fitting techniques. These analytical expressions along with the complete set of linear and quadratic temperature coefficients of DC and large-signal parameters calculated and presented in tabular form will be highly useful for designers and researchers to optimize the thermal design of the oscillators. Finally, the simulated results are found to be in close agreement with the experimentally measured data which validates the large-signal results presented in this paper.

References

[1] Acharyya A. Three-terminal graphene nanoribbon tunable avalanche transit time sources for terahertz power generation. Phys Status Solidi A, 2019, 216, 1900277

[2] Acharyya A. 1.0–10.0 THz radiation from graphene nanoribbon based avalanche transit time sources. Phys Status Solidi A, 2019, 216, 1800730

[3] Biswas A, Sinha S, Acharyya A, et al. 1.0 THz GaN IMPATT source: effect of parasitic series resistance. J Infrared, Millimeter Terahertz Waves, 2018, 39(10), 954

[4] Acharyya A. Gallium phosphide IMPATT sources for millimeter-wave applications. Iran J Electr Electron Eng, 2018, 14(2), 143

[5] Midford T A, Bernick R L. Millimeter Wave CW IMPATT diodes and oscillators. IEEE Trans Microwave Theory Tech, 1979, 27, 483

[6] Chang Y, Hellum J M, Paul J A, et al. Millimeter-wave IMPATT sources for communication applications. IEEE MTT-S International Microwave Symposium Digest, 1977, 1, 216

[7] Gray W W, Kikushima L, Morentc N P, et al. Applying IMPATT power sources to modern microwave systems. IEEE J Solid-State Circuits, 1969, 4, 409

[8] Acharyya A, Banerjee J P. Prospects of IMPATT devices based on wide bandgap semiconductors as potential terahertz sources. Appl Nanosci, 2014, 4, 1

[9] Eisele H. Selective etching technology for 94 GHz, GaAs IMPATT diodes on diamond heat sinks. Solid State Electron, 1989, 32(3), 253
[10] Tschernitz M, Freyer J. 140 GHz GaAs double-read IMPATT diodes. Electron Lett, 1995, 31(7), 582
[11] Berenz J J, Fank F B, Hierl T L. Ion-implanted p–n junction indium-phosphide IMPATT diodes. Electron Lett, 1978, 14(21), 683
[12] Yuan L, James A, Cooper J A, et al. Experimental demonstration of a silicon carbide IMPATT oscillator. IEEE Electron Device Lett, 2001, 22, 266
[13] Vassilevski K V, Zorenko A V, Zekentes K, et al. 4H-SiC IMPATT diode fabrication and testing. Technical Digest of International Conference on SiC and Related Materials, 2001, 713
[14] Mock P M, Trew R J. RF performance characteristics of double-drift MM-wave diamond IMPATT diodes. Proc of IEEE/Cornell Conf Advanced Concepts in High-Speed Semiconductor Devices and Circuits, 1989, 383
[15] Banerjee S, Acharyya A, Banerjee J P. Noise performance of heterojunction DDR MITATT devices based on Si~$Si_{1-x}Ge_x$ at W-band. Active and Passive Electronic Components, 2013, 2013, 1
[16] Banerjee S, Acharyya A, Banerjee J P, et al. Large-signal and noise properties of heterojunction DDR IMPATTs basd on $Al_xGa_{1-x}N$~GaN material system at 1.0 THz. Proceedings of 2nd International Conference on Foundations and Frontiers in Communication, Computer and Electrical Engineering (C2E2 – 2015), 2015
[17] Banerjee S, Acharyya A, Mitra M, et al. Large-signal properties of 3C-SiC/Si heterojunction DDR IMPATT devices at terahertz frequencies. Proceedings of the 34th PIERS, 2013, 462
[18] Luy J F, Casel A, Behr W, et al. A 90-GHz double-drift IMPATT diode made with Si MBE. IEEE Trans Electron Devices, 1987, 34, 1084
[19] Dalle C, Rolland P, Lieti G. Flat doping profile double-drift silicon IMPATT for reliable CW high power high-efficiency generation in the 94-GHz window. IEEE Trans Electron Devices, 1990, 37, 227
[20] Wollitzer M, Buchler J, Schafflr F, et al. D-band Si-IMPATT diodes with 300 mW CW output power at 140 GHz. Electron Lett, 1996, 32, 122
[21] Acharyya A, Chakraborty J, Das K, et al. Large-signal characterization of DDR silicon IMPATTs operating up to 0.5 THz. Int J Microwave Wireless Technol, 2013, 5, 567
[22] Acharyya A, Banerjee S, Banerjee J P. Effect of junction temperature on the large-signal properties of a 94 GHz silicon based double-drift region impact avalanche transit time device. J Semicond, 2013, 34, 024001
[23] Acharyya A, Goswami J, Banerjee S, et al. Quantum corrected drift-diffusion model for terahertz IMPATTs based on different semiconductors. J Comput Electron, 2015, 14, 309
[24] Sze S M, Ryder R M. Microwave avalanche diodes. Proc IEEE, 1971, 59, 1140
[25] Grant W N. Electron and hole ionization rates in epitaxial silicon at high electric fields. Solid State Electron, 1973, 16, 1189
[26] Canali C, Ottaviani G, Quaranta A A. Drift velocity of electrons and holes and associated anisotropic effects in silicon. J Phys Chem Solids, 1971, 32, 1707
[27] Electronic archive: new semiconductor materials, characteristics and properties. Available from: http://www.ioffe.ru/SVA/NSM/Semicond/index.html (Last accessed on: July 2019)
[28] Zeghbroeck B V. Principles of semiconductor devices. Colorado Press, 2011
[29] Varshini Y P. Temperature dependence of the energy gap in semiconductors. Physica, 1967, 34, 149
[30] Kern W, Puotinen D A. Cleaning solutions based on hydrogen peroxide for use in silicon semiconductor technology. RCA Rev, 1970, 31, 187
[31] Kugimiya K, Hirofuji Y, Matsuo N. Si-beam radiation cleaning in molecular-beam epitaxy. Jpn J Appl Phys, 1985, 24(5), 564
[32] Jorke H, Kibbel H. Doping by secondary implantation. J Electrochem Soc, 1986, 133, 774
[33] Iyer S S, Metzger R A, Allen F G. Sharp profiles with high and low doping levels in silicon growth by molecular beam epitaxy. J Appl Phys, 1981, 52(2), 5608
[34] Koenig U, Herzog H J, Jorke H, et al. Si-MBE with a high throughput of large diameter wafers. 2nd Int Symp MBE and Related Clean Surface Techniques (Tokyo), 1982, 193
[35] Casel A, Jorke H, Kasper E, et al. Dependence of hole transport on Ga doping in Si molecular beam epitaxial layers. Appl Phys Lett, 1986, 48, 922
[36] Acharyya A, Chatterjee S, Goswami J, et al. Quantum drift-diffusion model for IMPATT devices. J Comput Electron, 2014, 13, 739
[37] Acharyya A, Mukherjee M, Banerjee J P. Effects of tunnelling current on mm-wave IMPATT devices. Int J Electron, 2015, 102(9), 1429
[38] Acharyya A, Ghosh S. Dark current reduction in nano-avalanche photodiodes by incorporating multiple quantum barriers. Int J Electron, 2017, 104(12), 1957
[39] Dash G N, Pati S P. Small-signal computer simulation of IMPATT diodes including carrier diffusion. Semicond Sci Technol, 1991, 6, 348
[40] Acharyya A, Banerjee S, Banerjee J P. Influence of skin effect on the series resistance of millimeter-wave of IMPATT devices. J Comput Electron, 2013, 12, 511
[41] Acharyya A, Banerjee S, Banerjee J P. A proposed simulation technique to study the series resistance and related millimeter-wave properties of Ka-band Si IMPATTs from the electric field snapshots. Int J Microwave Wireless Technol, 2013, 5(1), 91
[42] Bandyopadhyay A M, Acharyya A, Banerjee J P. Multiple-band large-signal characterization of millimeter-wave double avalanche region transit time diode. J Comput Electron, 2014, 13, 769